Int. J. Heat Mass Transfer. Vol. 14, pp. 245–262. Pergamon Press Ltd. 1971. Printed in Great Britain

THE CALCULATION OF RADIATIVE HEAT FLUX IN A CYLINDRICAL FURNACE USING THE MONTE CARLO METHOD

F. R. STEWARD and P. CANNON

Department of Chemical Engineering, University of New Brunswick, Fredericton, New Brunswick, Canada

(*Received* 3 *September* 1969)

Abstract—The temperature profiles and heat flux distributions in an end-fired right cylindrical furnace with circumferential sink surfaces were calculated by the Monte Carlo Method, for various flow patterns. The combustion pattern was determined from precise experimental data taken on cold ducted jets and its calculation included the effect of turbulent fluctuations of the fuel and oxygen concentrations as well as the mean values.

The results compared favorably with previous calculations for identical conditions using the classical interchange method for the radiative terms. The Monte Carlo Method proved to be more flexible than the classical method in handling concentration variations in the radiating gases and changes in volume element geometry to conform more closely with jet structure. Various suggestions are proposed to circumvent the use of random numbers which lead to statistical errors, the major disadvantage of the Monte Carlo Method.

NOMENCLATURE

a_n, weighting factor for various gray gases contributing to the absorptivity of the real gas;

a'_n, weighting factor for various gray gases contributing to the emissivity of the real gas;

A, area of surface element [ft^2];

A_a, total radiant energy absorbed by a surface element per unit time [Btu/h];

A_{IN}, area of entrance end of furnace [ft^2];

A_T, total sink area of furnace [ft^2];

A''_V, total radiant energy absorbed by a volume element per unit time [Btu/h];

B_V, total sensible heat of gas flowing into a volume element per unit time [Btu/h];

c_p, heat capacity of the gases [Btu/lb°R];

C, convergence control coefficient;

C_a, net heat flux by convection to a surface element [Btu/h];

C_V, net heat flux by convection to a volume element [Btu/h];

Ct, Craya–Curtet number;

D_a, net heat flux by conduction to a surface element [Btu/h];

D_V, the heat generated by combustion within a volume element [Btu/h];

E_V, total sensible heat of gas flowing out of a volume element per unit time [Btu/h];

$f_{i,j}$, fraction of total combustion occurring in the volume element, i, j;

F_a, total radiant energy emitted by a surface element [Btu/h];

Fr, rate of energy release by combustion per sink area [Btu/hft^2 sink];

F_V, total radiant energy emitted by a volume element [Btu/h];

G, mass flow rate of gas normal to the heat transfer surface [lb/hft^2];

h, convection heat transfer, coefficient [Btu/hft^2];

i_I, momentum flux entering with the induced stream [ftlb/h^2];

i_N, momentum flux entering through the nozzle [ftlb/h^2];

K_n, absorption coefficient of a gray gas [ft^{-1}];
L, absorption path length [ft];
m_I, mass flow of induced stream [lb/h];
m_N, mass flow through nozzle [lb/h];
Nu, Nusselt number;
Pr, Prandtl number;
Re, Reynolds number;
T, temperature [°R];
u_d, dynamic mean velocity [ft/h];
u_k, kinematic mean velocity [ft/h];
U, jet velocity [ft/h];
V, volume of element [ft^3];
W, mass flow of gases into and out of volume elements [lb/h];
$\alpha(\ )$, absorptivity of the gas for radiant energy emitted at the temperature in parenthesis;
$\epsilon(\ )$, emissivity of the gas at the temperature in parenthesis;
ρ, density of gas [lb/ft^3];
σ, Stefan–Boltzmann constant [Btu/h ft^2 °R^4].

IN RECENT years many numerical methods have been proposed in order to solve the non-linear integro-differential equations resulting from radiative heat transfer problems. Of these methods the one which appears to be able to handle the complex situations which arise in actual engineering problems is the Monte Carlo Method. An extensive review of the use of this method in relation to heat transfer problems has recently been presented by Howell [1].

A number of radiative problems of increasing complexity which have been investigated by this method have recently appeared in the literature. These include; the radiative transfer within an infinite slab of gray gas between parallel walls [2], the same problem with a real gas [3], and [4], radiative transfer within a gray gas between concentric cylinders [5], the calculation of radiative interchange factors between surfaces whose properties are directional dependent [6], and the radiative transfer in a high temperature rocket nozzle [7] and [8].

It was felt that it would be worthwhile to carry out a numerical experiment using the Monte Carlo Method to analyze the radiative transfer in a realistic furnace chamber with a flow pattern and combustion pattern which could be calculated with reasonable accuracy. Such a problem is an end fired cylindrical furnace with heat absorbing circumferential walls and adiabatic end surfaces previously considered by Hottel and Sarofim [9] using a classical radiative interchange method. The radiative exchange for this problem has been simulated by the Monte Carlo Method for operating conditions similar to those used by Hottel and Sarofim in order to obtain a direct comparison of results. Additional modifications have been introduced so that the concentration of radiating (and absorbing) gases within the system may be taken into account. Also conical volume elements have been used to give a better representation of the jet flow pattern so that more accurate temperature and heat flow distributions may be obtained with less computation time.

Description of the system

The furnace under consideration, shown in Fig. 1, is an end fired right circular cylinder. In order to make a direct comparison with the work of Hottel and Sarofim [9] identical geometry was used. This consisted of a fixed length to diameter ratio of 8/3 and furnace diameters of 1 and 4 ft. The circumferential wall was taken as a gray sink maintained at 1460°R with an emissivity of 0·8. The end walls were treated as adiabatic surfaces with an emissivity of 0·5. Both types of surfaces were assumed to emit and reflect diffusely.

For convection heat transfer analysis the circumferential wall was assumed to consist of 4 in. dia. tubes backed by a refractory surface. The tube area was taken as equal to the circumferential wall.

The end walls are such that the gases may flow freely through them, but all radiation impinging on these surfaces is either absorbed and reradiated or reflected. This simplification defines a

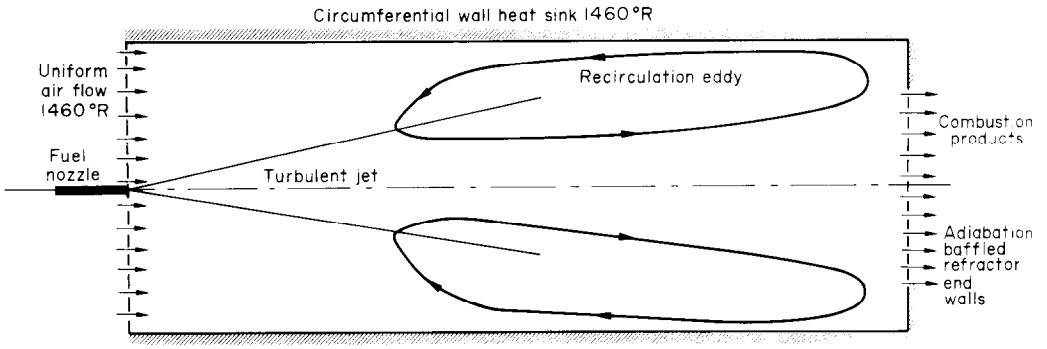

FIG. 1. The cylindrical furnace.

radiatively closed system and eliminates any complicating interaction with the entrance and exit systems.

The furnace was fired with a gaseous fuel of composition $(CH_2)_n$ having a heat of combustion of 19 150 Btu/lb. The air flow rate was maintained at 15 per cent excess air and was preheated to the temperature of the circumferential wall, 1460°R, so that furnace efficiencies could be calculated directly from the exit gas enthalpy. A summary of the range of system and calculation variables used is given in Table 1.

Division of the furnace enclosure

In order to perform a calculation of this nature it is necessary to divide the systen into a number of finite regions upon which an energy balance may be written.

Table 1. Summary of calculation variables

Length to diameter ratio	8/3
Furnace diameters	1.4 ft
Sink wall temperature	1460 R
Air and fuel preheat	1460 R
Fuel composition	$(CH_2)_n$ n = 3
Fuel Heat of Combustion	− 19150 Btu/lb
Excess air	15 per cent
Flow patterns	Plug flow, Ct numbers of 0·51, 0·18, 0·033
Firing rates	1×10^4 and 4×10^4* Btu/h/ft^2 of sink area
Axial division of furnace	8 equal elements
Radial division of furnace	3 and 6 cylindrical elements of equal width, also conical division to allow for concentration gradients.
Combustion patterns	As Sarofim [5] except for Ct = 0·51 where they were recalculated for different types of radial division

* Here the firing rates were slightly higher—up to 1 per cent higher than the nominal values above. In Sarofim's calculation [5] they were slightly lower—up to 1·5 per cent lower than the nominal values above.

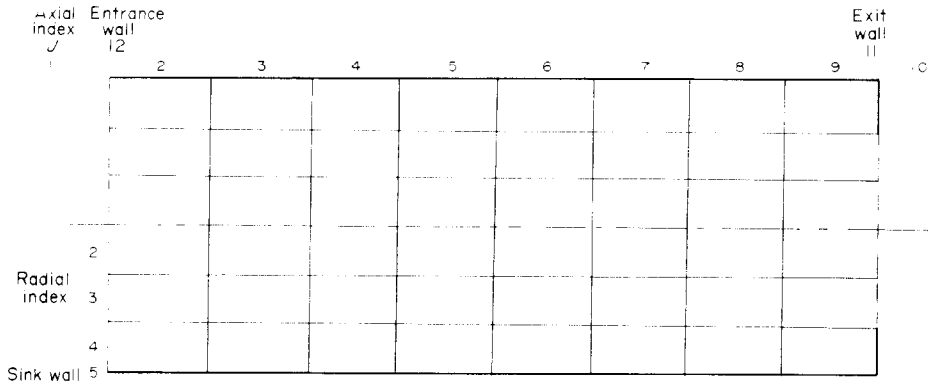

FIG. 2. Cylindrical radial division of the furnace into elements.

Initially the furnace enclosure was divided into elements identical to those used by Hottel and Sarofim [9] so that a direct comparison of the results could be made. This type of zoning included eight divisions of equal length along the axis and three divisions of equal increments along the radius. The surface elements corresponding to these divisions will include eight circumferential elements of equal width and three concentric elements on each end with equal incremental radii. The subscript j denotes the axial direction, and i the radial direction. The furnace divided in this manner is shown in Fig. 2.

In order to determine the effect of the size and shape of the volume elements on the calculation the system was later divided into six equal radial increments and finally three conical elements as shown in Fig. 3. In the latter instance the division between the radial element $i = 3$ and $i = 4$ was made to follow the jet boundary as closely as possible. The division between the element $i = 2$ and $i = 3$ bisected the remaining radius.

Energy balances

The temperature distribution and various heat fluxes within the system are determined by

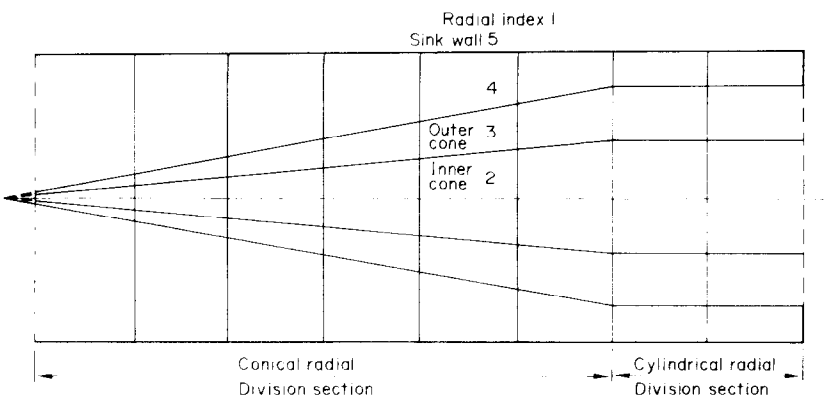

FIG. 3. Conical radial division of the furnace into elements.

writing energy balances on each of the individual surface and volume elements in the system.

Considering a volume element, V, a steady state energy balance can be broken down in the following manner:

A_v (the total radiant energy absorbed in V which was emitted by all surface and volume elements in the system including V itself),
$+ B_v$ (the total sensible heat content of gas flowing into V),
$+ C_v$ (the net heat flux by convection from the surface elements adjacent to V),
$+ D_v$ (the heat generated by combustion within V),
$- E_v$ (the total sensible heat content of gas flowing from V),
$- F_v$ (the total radiant energy emitted by V).

Writing a steady state energy balance on the surface element, A, in a similar manner:

A_a (the total energy absorbed by A which was emitted by all surface and volume elements in the system including A itself),
$+ C_a$ (the net heat flux by convection from volume elements adjacent to A),
$+ D_a$ (the net heat flux by conduction to A),
$= F_a$ (the total radiant energy emitted by A).

These energy balances result in a set of simultaneous equations equal to the total number of surface and volume elements within the system. Each equation contains one unknown which cannot be calculated by independent means. The unknowns are the temperature of the volume elements and the end wall surface elements. A solution can be obtained in principle since the number of equations just equals the number of unknowns. Each of the terms in the above equations were determined by a combination of theoretical considerations and available experimental data.

Furnace flow patterns

The calculation was carried out for four different flow patterns; plug flow and three flow patterns produced by a turbulent fuel jet fired at the centre of one end of the furnace.

The plug flow pattern was produced by the combustion products entering at the adiabatic flame temperature of the fuel–air mixture (4525°R) uniformly spread over the furnace entrance. The uniform flow proceeds along the furnace to the exit end but radial temperature gradients are allowed to develop.

The boundary conditions for the jet flow patterns include a finite diameter fuel jet at the centre of one end with the intake air uniformly spread over the remaining cross section. The burned exit gases pass through the centre portion of the adiabatic end wall included within a radius which is $\frac{2}{3}$ the furnace radius.

The flow characteristics of a turbulent ducted jet are known to be a function of the dimensionless group known as the Craya–Curtet number, Ct [10]. This analysis indicated that the flow pattern of such a system is given by the ratios of the mass and momentum fluxes of the jet and induced streams. High values of the Ct number indicated low nozzle momentum and sufficient ducted air to fulfil the jet entrainment requirements. When the Ct number becomes less than 0·74 the flow begins to recirculate from the downstream region of the jet along the duct wall to reenter the jetting stream since the induced air can no longer completely satisfy its entrainment requirements. The recirculation increases as the Ct number decreases until it fills the entire duct at $Ct = 0$. The three Ct numbers used were 0·033, 0·18 and 0·51 corresponding to recirculation rates of 9·5, 1·4 and 0·075 times the total exit flow rate respectively. Details of these flow patterns are given by Hottel and Sarofim [9] for identical Ct numbers and will not be presented here. It should be noted however, that the recirculation rate calculated here was 15 per cent lower than that of Hottel and Sarofim for a $Ct = 0·033$.

The cold flow patterns were used directly in the calculation. This assumption becomes more valid as the recirculating flow fills more of the

furnace since the temperature gradients are reduced. Beer *et al.* [11] found good agreement between flow patterns in a cold model and a hot furnace of similar geometry to the furnace under investigation.

The flows in the axial direction to and from each element of furnace volume were calculated by numerical integration of the axial velocity profiles. The net flows in the radial direction were then determined by a mass balance for each element. Details of the calculation including the computer program listing can be found in the original thesis [12].

The effective eddy flows in the radial direction have been calculated by Sarofim [13] using the cross-correlation $(\overline{U'T'}/U_{max}T_{max})$ for a free jet and the concentration and velocity profiles for a ducted jet reported by Becker [14]. The analogy between heat and mass transfer was assumed in using the concentration fluctuations to replace the temperature fluctuations in the above cross-correlation. The effective eddy flows used in the present calculation are those obtained by Sarofim [13]. These values have been interpolated graphically for the different types of radial diversions encountered in this analysis.

Once the flow pattern has been established it is possible to determine the sensible heat flux into and out of the volume elements, B_v and E_v, in terms of the temperatures of the surrounding elements and the element temperature itself. Thus, the sensible heat flowing into and out of the volume element i, j is given by:

$$B_v = \sum_{k=1}^{3 \text{ or } 4} W_{k \to i,j} c_p T_k \quad (1)$$

$$E_v = \sum_{k=1}^{3 \text{ or } 4} W_{i,j \to k} c_p T_{i,j} \quad (2)$$

where k is summed over the four (or three) volume elements surrounding the element i, j.

Fuel combustion and combustion product concentration distribution

The nozzle fluid concentration field and the axial values of the fluctuating component of nozzle fluid concentration for the cold ducted jet system measured by Becker [14] and [10] were used directly to calculate the distribution of the combustion of fuel within the furnace according to the method recommended by Hawthorne *et al.* [15]. The profiles of fuel concentration thus obtained were integrated numerically at each division to obtain the combustion occurring between fixed axial levels. The distribution of combustion between radial

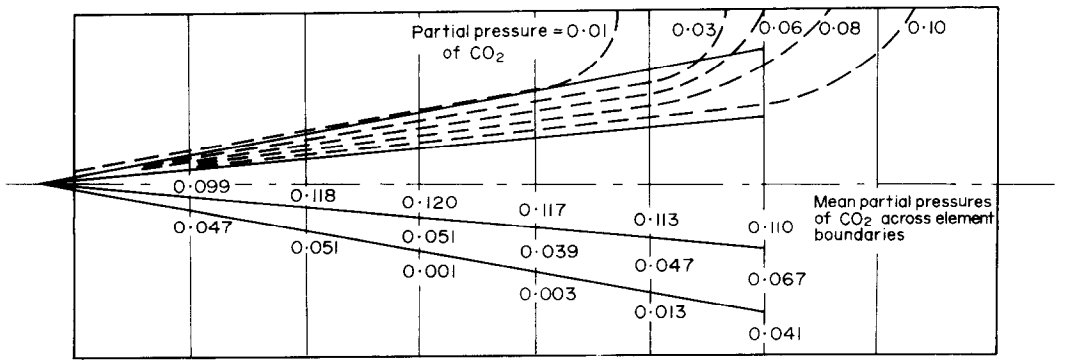

FIG. 4. Lines of equal CO_2 partial pressure and mean CO_2 partial pressures across element boundaries.

elements was estimated from mass balances on the radial elements.

The combustion patterns obtained in this manner are presented in Table 2 together with those calculated by Hottel and Sarofim [9]. There is some disagreement between the two calculations. The combustion patterns obtained by Hottel and Sarofim were used in the present calculation when the radiative heat transfer calculated by the Monte Carlo Method was to be compared directly with their results obtained from the classical interchange method. For all other calculations the combustion patterns obtained by the authors were used.

furnace into an inner cone region with a combustion partial pressure approximately double that of the outer cone region. A very low partial pressure of combustion product gases occurs in the region outside the cones. These conical divisions conform more closely to a jet structure and will be used to advantage in the radiative calculation.

The combustion patterns presented in Table 2 are used to evaluate D_v, the heat generated by combustion within each volume element according to the relation:

$$D_v = F_r A_T f_{i,j} \tag{3}$$

Table 2. Combustion patterns as fractions of the total combustion for each volume element

Axial index J =	2	3	4	5	6	7	8	9
Calculated in the present work for $Ct = 0{\cdot}51$								
3 Cylindrical radial divisions								
$I = 2$	0·138	0·230	0·181	0·141	0·140	0·083	0·057	0·030
6 Cylindrical radial divisions								
$I = 2$	0·140	0·137	0·091	0·048	0·044	0·030	0·019	0·010
$I = 3$	0·000	0·093	0·090	0·093	0·096	0·053	0·038	0·020
3 Conical radial divisions								
Inner cone $I = 2$	0·043	0·137	0·134	0·118	0·120	0·076	0·040	0·020
Outer cone $I = 3$	0·095	0·093	0·047	0·023	0·020	0·007	0·017	0·010
Calculated by Sarofim [13]								
3 Cylindrical radial divisions								
$Ct = 0{\cdot}51$ $I = 2$	0·185	0·170	0·160	0·130	0·105	0·100	0·080	0·070
$Ct = 0{\cdot}18$ $I = 2$	0·450	0·170	0·110	0·100	0·100	0·070	0·000	0·000
$Ct = 0{\cdot}33$ $I = 2$	1·000	0·000	0·000	0·000	0·000	0·000	0·000	0·000

A knowledge of the combustion pattern leads immediately to the combustion concentration field. Lines of constant carbon dioxide partial pressure are presented in Fig. 4. Since the fuel composition is $(CH_2)_n$ the water vapour partial pressure will be identical to that of CO_2 if the small difference in rate of final product formation is neglected. Also given in the same figure are the integrated values for each conical element. The figure shows that the conical radial divisions divide the first three quarters of the

where F_r = rate of energy release by combustion per sink area, Btu/hft^2 sink.
A_T = total sink area, ft^2
$f_{i,j}$ = fraction combustion in element i, j.

It is apparent that for a particular furnace geometry and Craya–Curtet number the combustion pattern is determined.

Convection heat transfer to the furnace walls

The convective heat transfer coefficients to the various elements of circumferential sink wall

were calculated as for flow parallel to 4 in. tubes using the correlation:

$$Nu = 0{\cdot}023\, Pr^{0{\cdot}4} Re^{0{\cdot}8} \tag{4}$$

The velocity at the wall at the entrance end of each axial element was substituted into the Reynolds number.

Thus the convection heat flux terms in the energy balances, C_r and C_a, can be written as:

$$C_r = hA(T_{i+1,j} - T_{i,j}) \tag{6}$$

$$C_a = hA(T_{i-1,j} - T_{i,j}) \tag{7}$$

where h can be obtained from Table 2.

Table 3. Convective heat transfer coefficients to the furnace side and end walls (Btu/h/ft² °R)

Furnace firing rate × 10 Btu/h/ft² sink	1	1	1	1	4	4	4
Furnace diameter, ft	1	4	4	4	4	4	4
Flow pattern	Plug	Plug			Plug		
Craya–Curtet number, Ct	0·051	0·051	0·18	0·033	0·51	0·18	0·033
Coefficient for end walls	2·18	2·18	2·18	2·18	6·42	6·42	6·42
Sarofim used	3·10	3·10	3·10	3·10	6·60	6·60	6·60
Coefficient for sink wall							
Axial index J							
2	1·5	1·5	1·5	1·5	1·5	1·5	1·5
3	1·5	1·5	1·5	1·5	1·5	1·5	2·87
4	1·5	1·5	1·5	1·62	1·5	1·5	4·90
5	1·5	1·5	1·5	2·27	1·5	1·5	6·88
6	1·5	1·5	1·5	2·64	1·5	1·5	8·01
7	1·5	1·5	1·5	2·57	1·5	1·63	7·79
8	1·5	1·5	1·5	2·24	1·5	1·58	6·79
9	1·5	1·5	1·5	1·85	1·5	1·5	5·61
Sarofim used J = 2–9	1·5	1·5	1·5	3·1	1·5	1·9	9·0

The convective heat-transfer coefficients to the surface elements on the end walls were determined by assuming flow normal to a flat plate. The relation presented by Friedman and Mueller [16]:

$$h = 0{\cdot}070\, G^{0{\cdot}78} \tag{5}$$

was used where G was taken as the average mass flow normal to the exit end wall, lb/hft² and h is given in English units, Btu/hft² °R.

A minimum value for h to all walls of 1·5 Btu/hft² °R was specified. These values differed somewhat from those used by Hottel and Sarofim [9] and the two sets are given in Table 3. The present calculation used those values calculated by the authors at all times and the values of Hottel and Sarofim are shown for comparison only.

Radiative heat fluxes

The terms which remain to be evaluated in the set of energy balances presented earlier are those associated with the radiative heat transfer A_r, A_a, F_v and F_a. In order to evaluate these terms the radiative properties of the combustion product gases were taken as identical to those used by Hottel and Sarofim [9]. They used a common technique which approximates a real gas by a mixture of gray gases where the emissivity is expressed as a weighted series of exponentials with different absorption coefficients which are independent of temperature. This approximation has been shown to be a good one [9].

$$\epsilon_g(T_g) = \sum_n a'_n(T_g)\,(1 - e^{-K_n L}) \tag{8}$$

where: $\sum_n a'_n(T_g) = 1$.

An expression based on similar assumptions for the absorptivity of the gas for radiation from a surface at a temperature, T_s, gives:

$$\alpha_g(T_s) = \sum_n a_n(T_s)(1 - e^{-K_n L}). \quad (9)$$

It has been shown [9] that a value of $n = 3$ represents accurately the gas mixture under consideration if the weighting factors variation with temperature is given by a third order polynomial such as:

$$a_n = a_{n0} + a_{n1}T + a_{n2}T^2 + a_{n3}T^3. \quad (10)$$

The values of the coefficients in the above equation for the system under consideration have been obtained by Hottel and Sarofim [9] and are given in Table B-1 of their paper.

The radiative emission of the volume element i, j can now be given directly as:

$$F_v = 4\sum_n a_n' K_n T_{i,j}^4 V \quad (11)$$

and the surface element i, j as:

$$F_a = \sum_n a_n T_{i,j}^4 A. \quad (12)$$

Substitution of the various terms into the original energy balances gives an equation for each element in terms of calculable quantities.

Volume Element i, j

$$4\sum_n a_n' K_n T_{i,j}^4 V = A_v + \sum_{k=1}^{3 \text{ or } 4} W_{k \to i,j} c_p T_k - \sum_{k=1}^{3 \text{ or } 4} W_{i,j \to k} c_p T_{i,j} + h_{i+1,j} A(T_{i+1,j} - T_{i,j}) + F_r A_T f_{i,j}. \quad (13)$$

Surface Element i, j

$$\sum_n a_n T_{i,j}^4 A = A_a + h_{i,j} A(T_{i-1,j} - T_{i,j}) + D_a. \quad (14)$$

The quantities in the above equations which remain to be determined are the radiative interchange terms A_v and A_a.

Monte Carlo simulation of radiative interchange

The classical method for handling radiative interchange between elements of volumes and/or surfaces is to evaluate the multiple integral which describes the interchange by some type of numerical integration technique. An alternative method used here is the simulation of the radiative emission in the enclosure by the Monte Carlo Method to obtain A_v and A_a directly.

The Monte Carlo Method uses bundles of energy to simulate the actual physical processes of radiant emission and absorption of energy occurring within the enclosure. These energy bundles are similar to photons in their behaviour, but the energy per bundle is constant and does not vary with the temperature, its spectral region or its point of emission. The energy per bundle is simply some fraction of the total or net radiant energy emitted throughout the system per unit time. The history of an energy bundle from its emission until it is finally absorbed is determined by a series of random numbers which are generated every time a decision with respect to position, direction, spectral region, path length, reflection or absorption is required.

Calculation procedure

The determination of the distribution of radiative emission throughout the enclosure requires a knowledge of the concentration of radiating gas and the temperature at each point in the system. The former was determined previously from the combustion and flow patterns; however, the temperature distribution is one of the unknown quantities sought. Therefore, a trial and error or iterative solution is necessary.

The calculation starts by assuming a temperature distribution among the volume elements so that the temperature dependent properties as well as the net radiant energy emitted by each element may be determined. This net radiant energy emitted by a volume element or an adiabatic end surface is given by

$$F_v - A_v = B_v + C_v + D_v - E_v \quad (15)$$

$$F_a - A_a = C_a + D_a \quad (16)$$

where the terms on the right-hand side can be obtained once the temperature of the element is assumed. Since the temperature of sink surfaces are fixed as a boundary condition, their total emission can be calculated directly from equation (12).

The radiative interchange among the elements, terms A_v and A_a, is obtained directly by the following Monte Carlo procedure. The net radiant energy emitted by all the volume and adiabatic surface elements, plus the total radiant energy emitted by the sink surface elements, is the radiative energy which must be simulated. This quantity is divided by the total number of energy bundles to be released in the simulation in order to obtain the energy per bundle. The net radiant energy emitted by an element (or the total radiant energy for a sink element) is divided by the energy per bundle to give the number of bundles originating at each element.

The bundles are now released from those elements with a positive number of bundles and traced until they are absorbed by either an element with a negative number of bundles or a sink surface with a fixed temperature. If the bundle is absorbed by an element with a net emission or an element which has already captured its required number of bundles, it is re-emitted as an initial emission at the point where it was absorbed.

The point of emission and path of travel is determined by random numbers in the following manner. The point of release within the volume element is determined by two random numbers giving its radial and axial position assuming that the origin of emission is equally likely at any point within the element. For gas radiation emission is equally likely in all directions and the circumferential and cone angles are determined by random numbers accordingly. The spectral range is given by another random number corresponding to the weighting factors, equation (8), which gives the absorption coefficient to be associated with this particular bundle. If the bundle does not fall within the clear spectral range an additional random number fixes the path length travelled before absorption according to the exponential law. The latter value gives the point on the surface where the bundle is intercepted or the location in the volume element where it is absorbed and possibly reemitted, in which case the procedure is repeated. All bundles are treated in this manner so that the total number of absorptions of each volume or surface element may be tabulated. The total number of bundles absorbed by each element including those reemitted multiplied by the energy per bundle gives the interchange of radiation among the elements, A_v and A_a.

Each of the above distributions involving a random selection is normalized and replaced by a rectangular distribution so that a single random number generator operating between zero and unity can be used in all cases. The distribution functions have been tabulated by Howell [1]. Additional details concerning the particular method used in this instance can be obtained from the original thesis [12].

A_v and A_a are now fixed quantities and a new temperature distribution can be calculated by solving the set of simultaneous equations (15) and (16), among the volume and surface elements. Since the element temperatures raised to the fourth power, the element temperatures raised to the first power and adjacent element temperatures raised to the first power are all present in each individual balance a solution was obtained by the Newton–Raphson method [17]. This new temperature distribution will be known henceforth as the "calculated temperatures", $T'_{ci,j}$. A new set of "assumed temperatures" $T'_{ai,j}$ is then obtained from the relation

$$T'_{ai,j} = \frac{T'_{ci,j} + CT_{ai,j}}{(C+1)} \tag{17}$$

where $T_{ai,j}$ is the previous set of assumed temperatures and C is the "convergence control factor" to be used systematically to promote rapid convergence.

Determination of efficient calculation parameters

In an iterative calculation of this type it is necessary to show that the solution is converging to the proper answer. It is desirable that the procedure should produce convergence as rapidly as possible. Extensive tests were conducted to give insight into various procedures for obtaining rapid convergence. Some typical results are presented in Figs. 5 and 6 for a one ft diameter furnace with a firing rate of 10^4 Btu/hft^2 sink undergoing plug flow. The volume elements were formed by eight axial and three cylindrical radial divisions. The points on the two figures are from the same calculation.

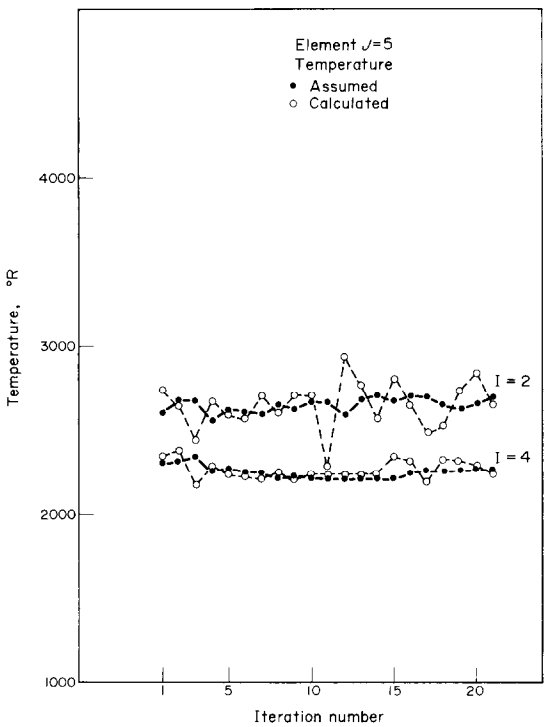

FIG. 5. Variation of assumed and calculated temperatures in converging to a final result. Plug flow with 3 cylindrical radial divisions.
Furnace diameter = 1 ft.
Firing rate = 1×10^4 Btu/h/ft^2 sink.

Figure 5 shows the values of the calculated temperature and assumed temperature for two volume elements $j = 5$, $i = 2$ and $j = 5$, $i = 4$, as the iteration proceeds; demonstrating the magnitude of the fluctuations encountered due to the random number simulation.

Figure 6 gives the average deviation of the new calculated temperatures from the previously assumed temperatures taken over all volume elements. This quantity is a measure of the accuracy of the temperature distribution once the calculation has converged.

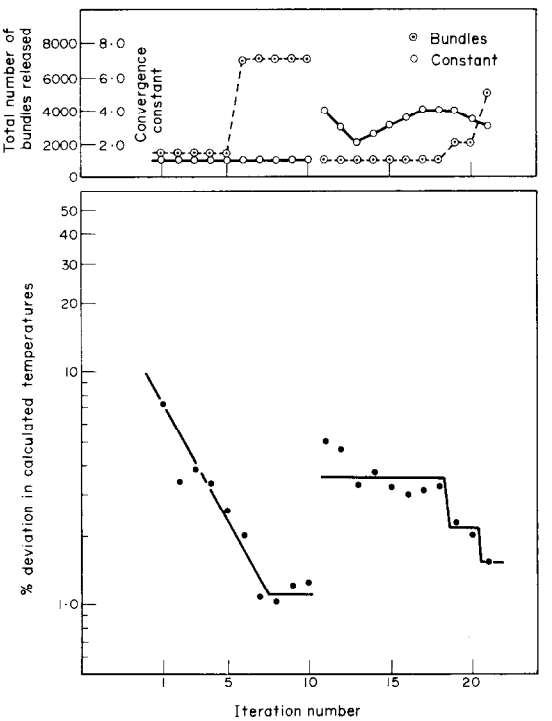

FIG. 6. The change in the gas temperature distribution accuracy as the calculation converges. Plug flow with 3 cylindrical radial divisions.
Furnace diameter = 1 ft.
Firing rate = 1×10^4 Btu/h/ft^2 sink.

Figures 5 and 6 indicate that when the number of bundles released in the Monte Carlo calculation is reduced (iteration 10) temperature fluctuations increase substantially.

Figure 6 indicates that the average temperature deviations decrease to a level determined by the number of bundles released. It was found [12] that this level is proportional to the number bundles released raised to the $\frac{1}{2}$ power as expected from theoretical considerations [1].

The computation time was found to be approximately proportional to the number of bundles released since following the paths of the bundles is the major source of repetitive calculation. In the run on which Figs. 5 and 6 are based it required about 3·5 s on the IBM 7094 machine to follow 1000 bundles. Thus, 10000 bundles would require approximately 35 s for tracing.

The only system parameter which influenced the computation time significantly was the furnace diameter. A four fold increase in the diameter from one to four ft increased the computation time for tracing 1000 bundles by approximately a factor of two. This is of course due to the increase in the number of absorptions and reemissions per bundle for the larger enclosure.

The rate of convergence is influenced by the convergence control coefficient where a high value gives slower convergence but a low value may cause instability when the radiative flux terms in equations (13) and (14) are small relative to the sensible heat terms. It appears from Fig. 6 that a value of unity is safe and a smaller value is justified as the sensible heat terms increase relative to the radiative heat flux terms.

Additional details on the effect of the convergence control coefficient and the number of bundles released may be obtained from the original thesis [12]. However, it can be stated that in general an efficient calculation with respect to computation time may be carried out by starting with a small number of energy bundles (1000) and a convergence control coefficient of unity. Once the temperature distribution reaches the level of accuracy associated with this particular number of bundles, the quantity should be increased by steps until the desired accuracy is obtained. Meanwhile the convergence control coefficient should be gradually decreased to zero.

Comparison with classical solution

A number of runs were made under similar conditions to those of Hottel and Sarofim [9] so that a direct comparison of the two methods could be made. Figures 7 and 8 present some typical results.

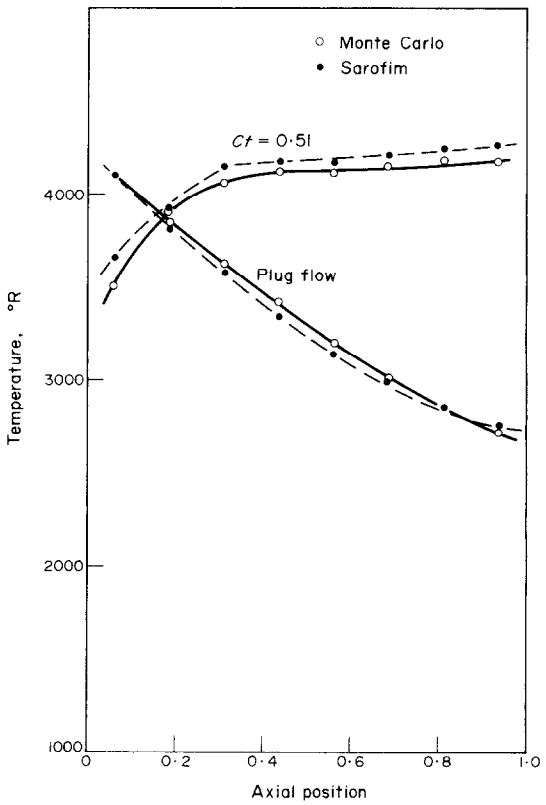

FIG. 7. Comparison of central radial element temperatures calculated with those of Sarofim. Combustion pattern of Sarofim and 3 cylindrical radial divisions.
Furnace diameter = 4 ft.
Firing rate = 4×10^4 Btu/h/ft^2 sink.

Figure 7 gives the axial temperature profile by both methods for the case of a 4 ft dia. furnace with a firing rate of 4×10^4 Btu/hft^2 sink surface. Results for plug flow and a Craya–Curtet number of 0·51 are shown. The furnace was divided into 8 axial and 3 radial cylindrical divisions for both cases. The combustion patterns calculated by Hottel and Sarofim, Table 2, were also used in the Monte Carlo calculation.

Figure 8 gives the heat flux distribution along the sink wall for plug flow with the same conditions by both methods. Other comparisons gave results with approximately the same magnitude of difference. Table 4 gives a break-down of the net heat flux to the sink for a number of test cases with some of the results of Hottel and Sarofim shown for comparison. The results from Figs. 7 and 8 and Table 4 indicate that the agreement between the two calculations is quite good. Only one case (furnace diameter 4 ft, firing rate 4×10^4 Btu/hft^2 sink, $Ct = 0{\cdot}033$) gives a total net heat flux which differs by more than 5 per cent between the two methods of calculation.

In the above Monte Carlo calculation the convection heat transfer coefficients calculated by the authors and presented in Table 2 were used at all times. The firing rates also varied slightly from the normal values as indicated in Table 4. An increase to six cylindrical radial divisions instead of three showed little difference in either the temperature or heat flux distributions for plug flow under identical conditions. However, a change to 6 divisions for $Ct = 0{\cdot}51$ gave a significant difference in the temperature distribution as indicated in Fig. 9, although the overall heat flux to the sink surface changed only

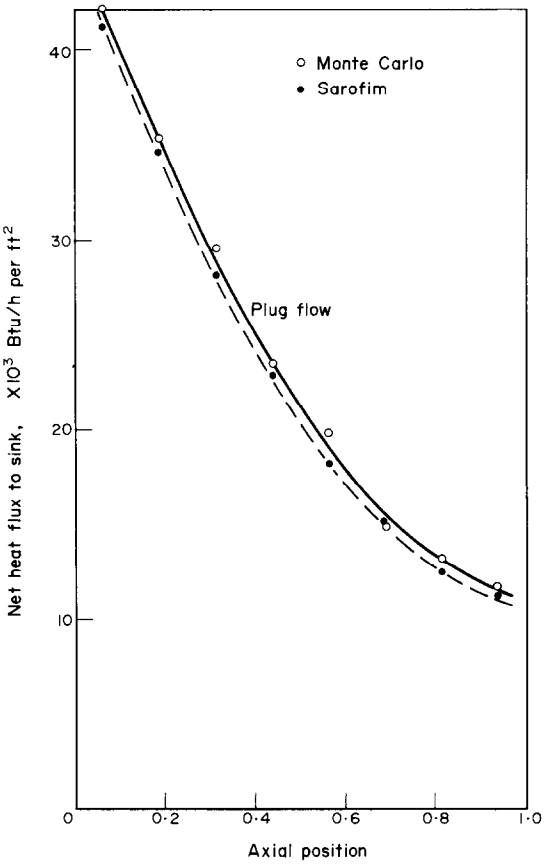

FIG. 8. Comparison of net heat flux to the sink wall calculated with that of Sarofim. 3 cylindrical radial divisions.
Furnace diameter = 4 ft.
Firing rate = 4×10^4 Btu/h/ft^2 sink.

Table 4. Net heat flux to circumferential sink wall

Dia. (ft)	Firing rate × 10 Btu/hft^2	Flow pattern	Radial div.	Net heat flux to sink wall (Btu/hft^2) Axial index J 2	3	4	5	6	7	8	9
1	1	Plug	3	16900	13300	9500	5980	4430	3240	2760	2490
1	1	Plug	6	16930	13150	9110	6340	4288	3402	2940	2289
4	1	Plug	3	21400	14000	8940	6030	4590	2640	1720	1760
4	1	Plug	6	21710	15330	8840	5492	3816	2702	2200	1971
4	1	0·51	3	3000	3806	4200	5770	6400	6445	6901	6870
4	1	0·51	Conical	2468	2982	4922	6818	6793	5553	5971	7104
4	1	0·18	3	3404	3957	4476	5790	6442	7754	7809	7581
4	1	0·033	3	4071	5806	6078	6589	7151	7380	7009	6945
4	4	Plug	3	42300	35500	29600	23400	19900	14800	13200	11700
4	4	Plug	6	42120	36060	28040	23810	18690	15240	13760	11150
4	4	0·51	3	2868	4120	6020	8649	12290	14960	18950	21100
4	4	0·51	Conical	3205	5407	7482	10200	12170	10860	17500	20390
4	4	0·18	3	4310	7060	13440	16960	19500	21000	21650	22210
4	4	0·033	3	11140	15670	19000	21700	22900	24100	23200	22200

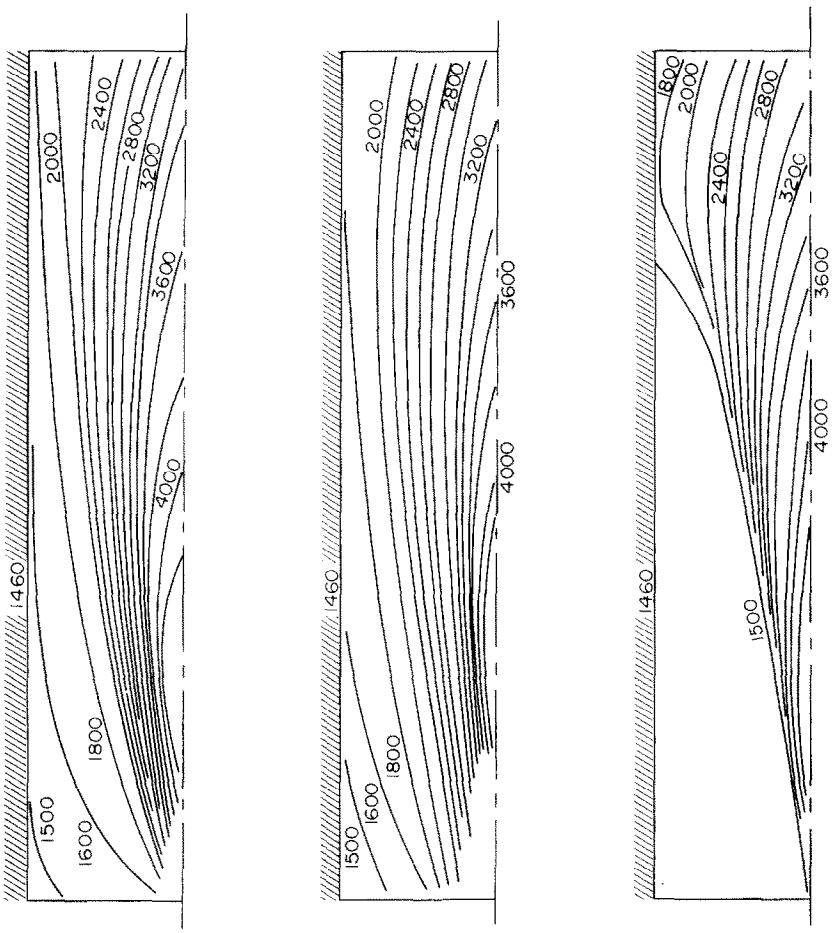

FIG. 9. The furnace temperature distribution °R.
Furnace diameter = 4 ft.
Firing rate = 1×10^4 Btu/h/ft^2 sink.

slightly. This indicates that when the jet structure is maintained throughout a significant section of the furnace other types of radial divisions should be considered.

Conical volume elements

The cylindrical volume elements used by Hottel and Sarofim [9] as well as in the above comparative calculations, are sufficient when plug flow or high recirculation rates are occurring. The same may be said for the assumption of a uniform combustion product concentration throughout the entire furnace enclosure. However, for small or zero recirculation the flow pattern is jet like in structure and cylindrical volume elements do not conform well to zones of uniform temperature and concentrations. The flow pattern and lines of constant partial pres-

sures of combustion products are rather conical in shape as shown in Fig. 4 for a Craya–Curtet number of 0·51 (small recirculation). Therefore, the furnace was divided into conical elements as shown in Fig. 3 to obtain more accurate results for approximately the same computation time. An additional refinement was introduced simultaneously by setting the centre cone partial pressure of carbon dioxide and water vapor each at 0·115 atm, and the concentric cone partial pressures of the same gases at one half that value. The gas surrounding the burning jet was taken as clear.

recirculation region seems to be significant as it also occurred for other firing rates. It is likely due to the flame jet cooling off as it progresses down the furnace. The higher values shown by the last two elements would seem to be given by the recirculation of hot gases with a high partial pressure of radiating gases near the wall as well as the proximity of the adiabatic end wall which reemits or reflects all the radiation impinging on it. The heat flux profiles for the same diameter and firing rate for two other Craya–Curtet numbers and plug flow are shown for comparison.

Table 5.

Convective heat flux to sink (Btu/hft^2)	(Sarofim)	Net radiant heat flux to sink (Btu/hft^2)	(Sarofim)	Total net heat flux to sink (Btu/hft^2)	(Sarofim)	Furnace heat Transfer Efficiency (%)
1290	(1253)	6050	(5990)	7360	(7243)	73·6
1090		6216		7306		73·1
950	(952)	6778	(6450)	7728	(7375)	77·3
810		6870		7680		76·8
472	(442)	4898	(4620)	5370	(5062)	53·7
185		5239		5424		54·2
718	(689)	5162	(5010)	5880	(5699)	58·8
1265	(1777)	5132	(6090)	6397	(7867)	64·0
2280	(2270)	21316	(20800)	23596	(23070)	59·0
2050		21168		23218		58·0
695	(705)	10361	(9846)	11056	(10545)	27·9
441		11060		11501		28·8
1640	(1933)	14084	(13720)	15724	(15653)	39·3
6920	(9630)	13068	(11100)	19988	(20730)	50·0

A comparison of the results obtained from conical and cylindrical radial divisions is given in Figs. 9 and 10. It is apparent that substantial differences occur. The temperature distribution given by conical divisions conforms more to that of a jet structure which is undoubtedly closer to reality. The heat flux distribution shows a markedly higher value near the entrance end of the furnace and somewhat lower value near the exit. The dip in the heat flux curve in the

Table 4 gives a break down of the heat flux distribution along with the overall heat fluxes both convective and radiative and the overall furnace efficiency. The overall efficiency is defined as the per cent of the energy which is released by combustion which is absorbed by the sink wall. These can be compared with similar efficiencies obtained by Hottel and Sarofim [9] from the classical interchange method of solution.

The computation time for each set of condi-

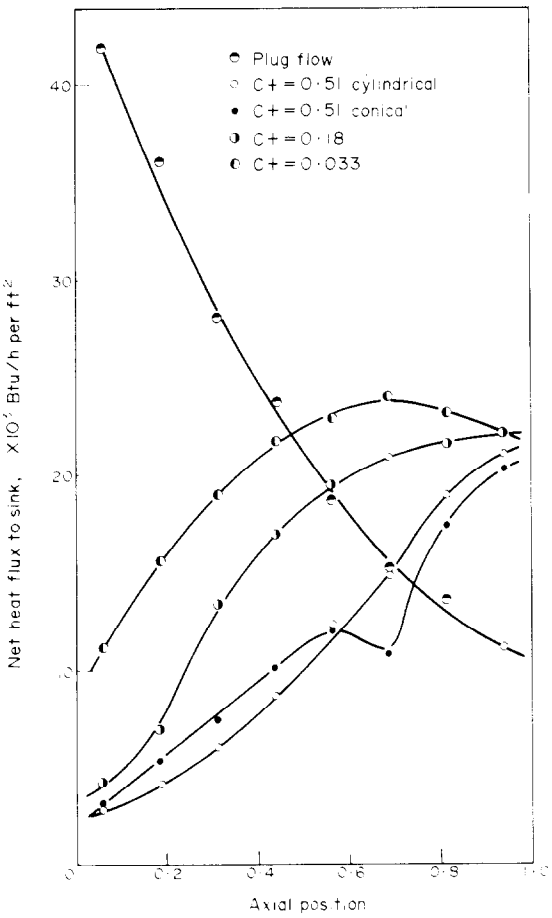

FIG. 10. Net heat flux distributions for various flow patterns.
Furnace diameter = 4 ft.
Firing rate = 4×10^4 Btu/h/ft^2 sink.

tions using the Monte Carlo Method is of the same order as that of the classical solution (approximately 2 min per run on the IBM 7094 for the Monte Carlo vs. 5 min per run on the IBM 709 for the classical). It should also be remembered that a set of rather extensive and tedious numerical integrations were required to obtain the interchange factors in preparation for the classical solution. No such calculation is necessary for the Monte Carlo simulation.

The Monte Carlo calculation needed only a slight modification when conical volume elements were introduced. For the classical solution it is necessary to repeat the preparatory numerical integrations to obtain an entirely new set of interchange factors. Even if this was done each concentration distribution of radiating gas would involve a separate set of such calculations. Additional refinements such as radiative scattering and directional radiative properties of surfaces are easily introduced into the Monte Carlo simulation. Either of these refinements would again require very substantial numerical preparation before the classical solution could be started, and then only a single example could be analysed from each set of preparatory calculations.

Improvements in the Monte Carlo Method

Although the Monte Carlo Method has very significant advantages over the classical interchange method for solving radiative transfer problems, it has one great disadvantage, dependence on random numbers. This dependence necessarily gives a certain statistical error in all quantities calculated. This error has been shown theoretically [1] to vary with the number of energy bundles released to the $\frac{1}{2}$ power.

In order to overcome this difficulty a modification of the Monte Carlo Method known as the Exodus Method has been recently proposed by Emery and Carson [18] for the solution of heat conduction problems. The Exodus Method replaces the random walk of the Monte Carlo Method with known probabilities so that a large number of bundles are traced simultaneously throughout a finite grid until practically all are absorbed (99·99 per cent or greater) by a wall. This method could be applied directly to radiative problems, but it has the serious drawback that the required probabilities must be calculated from the interchange factors between the volume and surface elements. This calculation is just the one that must be avoided if any substantial advantage is to be achieved by the Monte Carlo Method.

The idea that the decisions do not need to be taken in a random fashion is a useful one, however. For instance, the distribution of bundles

among the gray gases need not be randomly chosen but can be divided among the different coefficients according to the given fraction. Indeed it may be useful to divide the bundles so that one gray gas receives a larger number of lower energy bundles because a more accurate calculation is warranted.

Similarly, when a bundle strikes a surface its absorption or reflection need not be determined randomly since one can take every second or third bundle as reflected according to the surface reflectivity. It is also possible to visualize a non-random process for the determination of geometric quantities by initiating an equal number of bundles at a set of points distributed evenly throughout each volume element where an equal number of these same bundles would be emitted in a certain fixed number of evenly distributed directions. The number of bundles absorbed in each element along the path would be determined by the exponential absorption law. In this manner all random decisions can be replaced by calculable ones. The feasibility of this method needs further investigation.

Conclusions

(1) The Monte Carlo Method has been shown to compare favorably with the classical interchange method in respect to computation time for determining the radiative heat flux and temperature profile in a furnace enclosure where flow and combustion patterns are taken into account.

(2) It was shown that the Monte Carlo Method is considerably more flexible in dealing with rapidly varying temperature and radiating gas concentration profiles since the volume geometry can be changed with only slight modifications in procedure. Thus as the problem becomes more sophisticated it appears that the Monte Carlo Method becomes more advantageous. It would also appear worthwhile to investigate the use of a modified version of the Exodus Method in order to eliminate the statistical error due to the random nature of the Monte Carlo Method.

ACKNOWLEDGEMENTS

The authors are grateful to the National Research Council of Canada who provided financial support for this work.

The computer calculations were carried out at the Computation Centre of the University of New Brunswick and later at the Institute of Computer Science of the University of Toronto by special agreement.

REFERENCES

1. J. R. HOWELL, Application of Monte Carlo to heat transfer problems, *Advances in Heat Transfer*, Vol. 5, pp. 1–54. Academic Press, New York (1968).
2. J. R. HOWELL and M. PERLMUTTER, Monte Carlo solution of thermal transfer through radiant media between gray walls, *J. Heat Transfer* **86**, 116 (1964).
3. J. R. HOWELL and M. PERLMUTTER, Monte Carlo solution of radiant heat transfer in a nongray nonisothermal gas with temperature dependent properties, *A.I.Ch.E. Jl* **10**, 562 (1964).
4. P. M. CAMPBELL, Monte Carlo Method for radiative transfer, *Int. J. Heat Mass Transfer* **10**, 519 (1967).
5. M. PERLMUTTER and J. R. HOWELL, Radiative transfer through a gray gas between concentric cylinders using Monte Carlo, *J. Heat Transfer* **86**, 169 (1964).
6. J. S. TOOR and R. VISKANTA, A numerical experiment of radiative heat interchange by the Monte Carlo method, *Int. J. Heat Mass Transfer* **11**, 883 (1968).
7. J. R. HOWELL, M. K. STRITE and H. RENKEL, Heat transfer analysis of rocket nozzles using very high temperature propellants, *AIAA Jl* **3**, 669 (1965).
8. J. R. HOWELL, M. K. STRITE and H. RENKEL, Analysis of heat transfer effects in rocket nozzles operating with very high temperature hydrogen, NASA Tech. Rept. TR R-220, (1965).
9. H. C. HOTTEL and A. F. SAROFIM, The effect of gas flow patterns on radiative transfer in cylindrical furnaces, *Int. J. Heat Mass Transfer* **8**, 1153 (1965).
10. H. A. BECKER, H. C. HOTTEL and G. C. WILLIAMS, Mixing and flow for ducted turbulent jets. *Ninth Symposium International on Combustion*, 7–20. Academic Press, New York (1963).
11. J. M. BEER, N. A. CHIGIER and K. B. LEE, *Ninth Symposium International on Combustion*, 892–900. Academic Press, New York (1963).
12. P. CANNON, The calculation of radiative heat flux in furnace enclosures using the Monte Carlo Method, M.Sc. Thesis, Chem. Eng. Dept., University of New Brunswick, Fredericton, New Brunswick (1967).
13. A. F. SAROFIM, Radiant heat transmission in enclosures, Sc.D. Thesis, Chem. Eng. Dept. M.I.T. (1962).
14. H. A. BECKER, Concentration fluctuations in ducted jet mixing, Sc.D. Thesis, Chem. Eng. Dept., M.I.T. (1961).
15. W. R. HAWTHORNE, D. S. WEDDELL and H. C. HOTTEL, Mixing and combustion in turbulent gas jets, *Third Symposium on Combustion and Flame Explosion Phenomium*, p. 249. Williams and Wilkins, Baltimore (1949).
16. S. J. FRIEDMAN and A. C. MUELLER, Heat transfer to flat surfaces, Proceedings of the General Discussion on Heat Transfer, New York, pp. 138–42 (1951).

17. L. LAPIDUS, *Digital Computation for Chemical Engineers* pp. 288–92. McGraw-Hill, New York (1962).
18. A. F. EMERY and W. W. CARSON, A modification to the Monte Carlo method–The Exodus Method, *J. Heat Transfer* **90**, 328 (1968).

CALCUL PAR LA MÉTHODE DE MONTE CARLO DU FLUX THERMIQUE RAYONNANT DANS UN FOUR CYLINDRIQUE

Résumé—Les profils de température et les distributions du flux thermique dans un four cylindrique avec combustion à une extrémité et avec des surfaces-puits circonférentielles, sont calculés par la méthode de Monte Carlo pour différents types d'écoulement. La figure de combustion est déterminée à partir d'essais expérimentaux précis sur des jets froids guidés et son calcul comprend l'effet de fluctuations turbulentes des concentrations en combustible et oxygène aussi bien que les valeurs moyennes.

Les résultats correspondent de facon satisfaisante aux calculs faits pour des conditions identiques utilisant la méthode d'interchange classique pour les termes de rayonnement. La méthode de Monte Carlo est plus flexible que la méthode classique en tenant compte des variations de concentration dans les gaz rayonnants et des changements dans la géométrie volumique de l'élément, pour se conformer plus étroitement à la structure du jet. Des suggestions sont proposées pour éviter l'utilisation des nombres au hasard qui conduisent à des erreurs statistiques, le plus gros désavantage de la méthode de Monte Carlo.

BERECHNUNG DES WÄRMETRANSPORTES DURCH STRAHLUNG IN EINEM ZYLINDRISCHEN OFEN, NACH DER MONTE-CARLO-METHODE

Zusammenfassung—Nach der Monte-Carlo-Methode wurden die Temperaturprofile und Wärmeflussverteilungen in einem endbefeuerten zylindrischen Ofen berechnet, der konzentrisch umgeben ist von Oberflächen die als Senke wirken. Verschiedene Strömungsmuster sind berücksichtigt. Das Verbrennungsmuster wurde aus genauen experimentellen Daten ermittelt, die an kalt betriebenen Düsen aufgenommen worden waren. Die Berechnung der Muster schloss sowohl den Effekt von turbulenten Fluktuationen der Brennstoff- und Sauerstoffkonzentrationen als auch die Mittelwerte ein.

Die Ergebnisse lassen sich sehr gut mit früheren Berechnungen für identische Bedingungen vergleichen, wobei die klassische Austauschmethode für die Strahlungsterme verwendet worden war. Die Monte-Carlo-Methode erwies sich flexibler als die klassiche Methode in der Behandlung von Konzentrationsänderungen in den strahlenden Gasen und von Änderungen der Geometrie des Volumenelementes. Diese Änderungen sollten bessere Übereinstimmung mit der Strahlenstruktur gewährleisten.

Es wurden verschiedene Vorschläge gemacht,um die Benutzung von Zufallszahlen, die zu statistischen Fehlern führt und die der Hauptnachteil der Monte-Carlo-Methode ist, zu umgehen.

ПРИМЕНЕНИЕ МЕТОДА МОНТЕ-КАРЛО ДЛЯ РАСЧЕТА ЛУЧИСТОГО ТЕПЛОВОГО ПОТОКА В ЦИЛИНДРИЧЕСКОЙ ПЕЧИ

Аннотация—Методом Монте-Карло рассчитаны для различных типов течения профили температуры и распределения тепловых потоков в прямой цилиндрической печи со стоками на боковой поверхности и топкой в торце. Режим горения определялся на основании точных экспериментальных данных, полученных для холодных струй в каналах. В расчете наряду со средними значениями концентраций топлива и кислорода учитывалось влияние их турбулентных пульсаций.

Результаты хорошо согласуются с известными расчетами лучистого теплообмена, выполненными классическими методами. Метод Монте-Карло оказался более приемлемым (по сравнению с классическими) для учета изменений концентрации в излучающих газах и изменений геометрии элемента объема для более близкого соответствия со структурой струй. Предложены различные варианты, позволяющие избежать использования случайных чисел, приводящих к статистическим омибкам, что является основным недостатком метода Монте-Карло.